# A Full Rheological Characterization of a Low-density Polyethylene Melt in Controlled Elongational Flows

Manfred H. Wagner and Víctor Hugo Rolón-Garrido

Chair of Polymer Engineering/Polymer Physics, Berlin Institute of Technology (TU Berlin), Fasanenstrasse 90, D-10623 Berlin, Germany

Correspondence to: Manfred H. Wagner (E-mail: *manfred.wagner@tu-berlin.de*)

**ABSTRACT**

We present a full experimental characterization of the long-chain branched polyethylene melt 1840D in controlled elongational flows, thereby confirming the results of an earlier investigation. Experiments were performed at constant elongation rate, constant tensile stress and constant tensile force by use of a Sentmanat Extensional Rheometer (SER) in combination with an Anton Paar MCR301 rotational rheometer. Experimental limitations and the accessible experimental window are discussed. The Wagner I model was used to model the experimental data. Predictions of the steady-start elongational viscosity in constant strain rate and creep experiments are found to be identical, albeit only by extrapolation of the experimental data to Hencky strains of the order of 6. For constant stress experiments, a minimum in the strain rate and a corresponding maximum in the elongational viscosity are found at a Hencky strain of the order of 3, and the elongational viscosity at the maximum, although larger than the steady-state value, follows roughly the general trend of the steady-state elongational viscosity. The constitutive analysis also shows that constant tensile force experiments reveal a larger strain hardening potential than seen in constant elongation rate or constant tensile stress experiments. This may be indicative of the effect of necking under constant elongation rate or constant tensile stress conditions according to the Considère criterion.

**KEYWORDS**: Rheology, MSF model, elongational flow, strain hardening, low-density polyethylene, polymer melts, constant elongational rate, constant stress, creep, constant force

**AUTHOR BIOGRAPHIES**

Manfred H. Wagner is Professor for Polymer Engineering and Polymer Physics at TU Berlin. His scientific interests include constitutive equations for polymeric systems, the application of rheology to polymer processing, and structure-property relations for polymers. He has published to date over 250 papers on solid state physics, carbon and graphite technology, and rheology and processing of polymer melts. He received the Annual Award 1981 of the British Society of Rheology, the Swinburne Award of The Institute of Materials in 2002, and the Weissenberg Award of the European Society of Rheology in 2011.

Víctor Hugo Rolón-Garrido was born in México. After studying physics and mathematics in México City, he graduated in Berlin, Germany, as M.Sc. in Polymer Science and obtained his PhD under the supervision of Prof. Manfred H. Wagner. He is interested in the quantitative description of experimental results through constitutive equations, and in structure-properties relations of polymer melts and solutions. He is member of the Mexican National System of Researchers.

**INTRODUCTION**

Recently, we have analyzed the rheology of the low-density polyethylene (LDPE) melt 3020D in elongational flow at constant elongation rate, constant tensile stress and constant tensile force[1]. Here, we present a full rheological characterization of another LDPE melt, LDPE 1840D, in controlled elongational flows, with the intention to confirm the results of our earlier investigation.

Elongational flow at constant rate conditions is widely used to characterize structural features of polymer melts such as long-chain branching[2-5], and efforts have been made to relate this type of rheological characterization to the performance in polymer processing operations such as fiber spinning, blow molding, thermoforming, film blowing, and foaming[6-10], although most of these processes take place under the condition of constant engineering stresses.

Tensile creep experiments, i.e. elongational experiments at the condition of constant true tensile stresses, have also been reported, and comparison of steady-state elongational viscosities measured at constant stress and constant elongation rate[11-14], creep and creep recovery data[15-18], as well as failure and rupture mechanisms[19] have been presented.

Elongation at constant engineering stress, i.e. "constant force elongation", is of great industrial relevance, since it is the correct analogue of steady fiber spinning as e.g. exemplified by the so-called Rheotens test[20-23]: In fiber spinning at constant draw-down force, a material element experiences the same deformation condition in a spatial (Eulerian) reference frame as a material element in constant force elongational flow, i.e. fiber spinning is the Eulerian equivalent of Lagrangian constant force elongational flow[24]. Therefore, while elongational flow at constant strain rate and constant stress conditions allows the determination of well-defined material

functions such as tensile stress growth coefficient and tensile creep compliance, constant force elongation represents an important test condition in its own right for polymer melt characterization in relation to processing behavior. Constant force extension has been the subject of several theoretical analyses[24-27]. However, to the best knowledge of the authors, the only works presenting a comparison of experimental data of constant force elongation of polymer melts to predictions of a constitutive equation was presented by Raible et al.[28] 30 years ago, and recently by Wagner and Rolón-Garrido[1,29].

The experiments to be reported here were performed by use of the Sentmanat Extensional Rheometer (SER)[30] in combination with the Anton Paar MCR301 rotational rheometer in three different elongation modes: constant strain rate, constant stress and constant tensile force. We present experimental data for the long-chain branched polyethylene melt 1840D. To analyze and compare the experimental data, we use the Wagner I equation, i.e. the damping function approach[31].

## EXPERIMENTAL DATA

The linear-viscoelastic characterization of LDPE 1840D and a master curve at the reference temperature of 170°C have been reported earlier[5]. The partial relaxation moduli $g_i$ and relaxation times $\lambda_i$ as well as the (calculated) zero-shear viscosity $\eta_0$ are presented in Table 1 together with the molecular characterization of the melt.

To perform elongational deformations, a Sentmanat Extensional Rheometer (model SER2-P universal testing platform from Xpansion Instruments) was used, which is a dual windup extensional rheometer tailored to an Anton Paar MCR301 rheometer equipped with a CTD450 convection oven. The protocol for correcting the effects of thermal expansion and of pre-stretch to minimize sagging is described elsewhere[5]. All elongational experiments were performed at 170°C. The constant elongation rate data of LDPE 1840D are the ones presented by Rolón-Garrido et al.[5]. For the constant stress elongational experiments, the true stress $\sigma_0$ was kept

constant in the range between 5,000 and 70,000 Pa. In the case of the constant force elongational experiments, the value of the torque *M*, which is proportionally to the tensile force *F* according to

$$\sigma_0 = \frac{M}{2RA} = \frac{F}{A} \tag{1}$$

was the variable kept constant so that the engineering stress $\sigma_0$ is in the range between 5,000 and 70,000 Pa. $R$ is the radius of the drums and $A$ the cross-sectional area of the sample at room temperature. Note that although we report the engineering stress at room temperature in the following, due to thermal expansion the engineering stress at the measuring temperature *T=170°C* is reduced by a factor $\left(\frac{\rho}{\rho_0}\right)^{2/3} = 0.84$, where $\rho_0$ the density of the sample at room temperature and $\rho$ the melt density of the polymer at *T=170°C*[32,33].

Because the experiments were stopped before one full revolution of the drums, i.e. before the sample is wound up onto itself, the maximum accessible Hencky strain $\varepsilon$ is limited to $\varepsilon < 4$. Two to five measurements per elongational rate, constant true stress or engineering stress were performed to verify reproducibility of the tests. The test conditions were thus equivalent to the test conditions used in our earlier work[1] on LDPE melt 3020D.

**THEORY**

For simplicity and for comparison with earlier results of Raible et al.[28], the constitutive equation used here is the so-called Wagner-I model[34]

$$\underline{\underline{\sigma}}(t) = \int_{-\infty}^{t} \overset{\circ}{m}(t-t')h(I_1, I_2)\underline{\underline{C}}_t^{-1}(t')dt' \tag{2}$$

which was also in our earlier work[1] on LDPE 3020D and is summarized here for the convenience of the reader. $\underline{\underline{\sigma}}(t)$ is the extra stress tensor, and $\overset{\circ}{m}(t-t')$ is the memory function related to the

linear-viscoelastic relaxation modulus $\overset{\circ}{G}(t)$, which will be represented in the following by a sum of the discrete relaxation modes given in Table 1,

**TABLE 1.** Molecular characterization and relaxation spectrum of LDPE 3020D obtained by dynamic shear measurement at a reference temperature of 170°C[5]

| LDPE 1840D | |
|---|---|
| $M_w$=490 kg/mol | |
| $M_n$=16 kg/mol | |
| $M_w/M_n$=30.6 | |
| $T_m$=110°C | |
| $\eta_0 = 2.133x10^5\, Pa \cdot s$ | |
| $g_i$ (Pa) | $\lambda_i$ (s) |
| $1.819x10^5$ | $7.922x10^{-4}$ |
| $6.192x10^4$ | $5.241x10^{-3}$ |
| $3.968x10^4$ | $2.446x10^{-2}$ |
| $2.437x10^4$ | $1.132x10^{-1}$ |
| $1.438x10^4$ | $5.190x10^{-1}$ |
| $7.518x10^3$ | $2.455x10^0$ |
| $3.665x10^3$ | $1.170x10^1$ |
| $1.347x10^3$ | $1.041x10^2$ |

$$\overset{\circ}{m}(t-t') = \frac{d\,\overset{\circ}{G}(t-t')}{dt'} = \sum_{i=1}^{N}\left(\frac{g_i}{\lambda_i}\right)e^{\frac{-(t-t')}{\lambda_i}} \tag{3}$$

The relative Finger tensor $\underline{\underline{C}}_t^{-1}(t')$ takes into account affine deformations of material lines. The damping function $h(I_1, I_2)$, which depends on the first and second invariant $I_1$ and $I_2$ of the Finger tensor, expresses the loss of connectivity in the structure of the temporary polymer network due to deformation[34,35]. For a review on the concept of damping functions in rheology see Rolón-Garrido and Wagner[31].

This model has already been applied previously to study constant tensile force experiments[28,35]. The particular choice of the model is not critical for the analysis of the experimental data presented in the following, as long as the model does provide an accurate description of material behaviour. In uniaxial extension and based on experimental data of a LDPE melt, the damping function $h_u$ can be expressed as[36]

$$h_u(\varepsilon) = \left[a\exp(2\varepsilon) + (1-a)\exp(m\varepsilon)\right]^{-1} \tag{4}$$

For typically values of the parameter $a<<1$ and of the parameter $m<<2$, $m$ represents the slope of the damping function at small and medium Hencky strains $\varepsilon$. The parameter $a = \exp(-2\varepsilon_0)$ defines the Hencky strain $\varepsilon_0$ at which the transition to a steady-state elongational viscosity begins. For constant elongation rate experiments, the true stress $\sigma(t)$ is given by

$$\sigma(t) = \int_{-\infty}^{t} \overset{\circ}{m}(t-t')h_u(\varepsilon_{t,t'})\left[\exp(2\varepsilon_{t,t'}) - \exp(-\varepsilon_{t,t'})\right]dt' \tag{5}$$

$\varepsilon_{t,t'}$ is the relative Hencky strain $\varepsilon(t)-\varepsilon(t')$ between times $t$ and $t'$, which for a constant strain rate $\dot{\varepsilon}$ is prescribed as $\varepsilon_{t,t'} = \dot{\varepsilon}(t-t')$. For constant strain rate flows, the integral can be inverted, and the damping function can be calculated from experimental data obtained in constant elongation rate flow starting at time $t=0$ by[36]

$$h_u(\varepsilon) = \frac{\dfrac{\sigma(\varepsilon)}{\overset{\circ}{G}(\varepsilon/\dot{\varepsilon})} - \dfrac{1}{\dot{\varepsilon}}\displaystyle\int_0^{\varepsilon}\sigma(\varepsilon')\frac{\overset{\circ}{m}(\varepsilon'/\dot{\varepsilon})}{\left(\overset{\circ}{G}(\varepsilon'/\dot{\varepsilon})\right)^2}\,d\varepsilon'}{\exp(2\varepsilon)-\exp(-\varepsilon)} \tag{6}$$

For constant stress experiments starting at time $t=0$, the true stress $\sigma(t)$ is constant,

$$\sigma(t) = \sigma_0 = \int_{-\infty}^{t} \overset{\circ}{m}(t-t')h_u(\varepsilon_{t,t'})\left[\exp(2\varepsilon_{t,t'}) - \exp(-\varepsilon_{t,t'})\right]dt' \tag{7}$$

In this case, the left hand side of Eq.(7) is prescribed, and the Hencky strain $\varepsilon(t)$ can be calculated from Eq.(7) by a numerical inversion routine, the details of which have been reported earlier[36].

For constant tensile force experiments starting at time *t=0*, the true stress increases with the deformation according to

$$\sigma(t) = \sigma_0 \exp(\varepsilon(t)) = \int_{-\infty}^{t} \overset{\circ}{m}(t-t') h_u(\varepsilon_{t,t'}) \left[\exp(2\varepsilon_{t,t'}) - \exp(-\varepsilon_{t,t'})\right] dt' \tag{8}$$

The unknown Hencky strain $\varepsilon(t)$, which appears on the left and the right side of Eq.(8) can again be calculated by a similar numerical inversion routine[36].

At first instant, a viscoelastic material suddenly subjected to a tensile stress reacts elastically, i.e. at time $t = 0$, the strain rate $\dot{\varepsilon}$ is infinite. Immediately after the elastic step, i.e. at time $t = 0+$, the strain rate is given by[24, 28]

$$\dot{\varepsilon}(t=0+) = \frac{\sigma_0 \sum_i \frac{g_i}{\lambda_i}}{\left(\sum_i g_i\right)^2 \left[\Lambda(t=0+) + 2\Lambda(t=0+)^{-2}\right]} \tag{9}$$

$\Lambda(t=0+)$ is the relative stretch after the elastic step-strain deformation, which can be approximated for small $N$ by

$$\Lambda(t=0+) = 1 + N + N^2 + \ldots \tag{10}$$

with

$$N = \frac{\sigma_0}{3\sum_i g_i} \tag{11}$$

## RESULTS AND DISCUSSION

### Experiments at Constant Elongational Rate

Elongational viscosities determined for LDPE 1840D at constant elongation rates are presented together with the predictions of the constitutive model according to Eq.(2) in Figure 1. The nonlinear parameters used are summarized in Table 2. It is seen that the model allows for an excellent representation of the experimental data for all elongation rates investigated.

The experimentally determined damping function as calculated from the constant elongation rate data by use of Eq.(6) are shown in Figure 2, which proofs that the data are perfectly time-deformation separable in the experimental window accessible, i.e. up to a Hencky strain of roughly 3.5.

**TABLE 2** Nonlinear parameters fitted to constant tensile force and constant strain rate data.

| Sample | *m* | $\varepsilon_0$ at constant force | $\varepsilon_0$ at constant strain rate / constant true stress |
|---|---|---|---|
| LDPE 1840D | 0.38 | 2.76 | 2.44 |

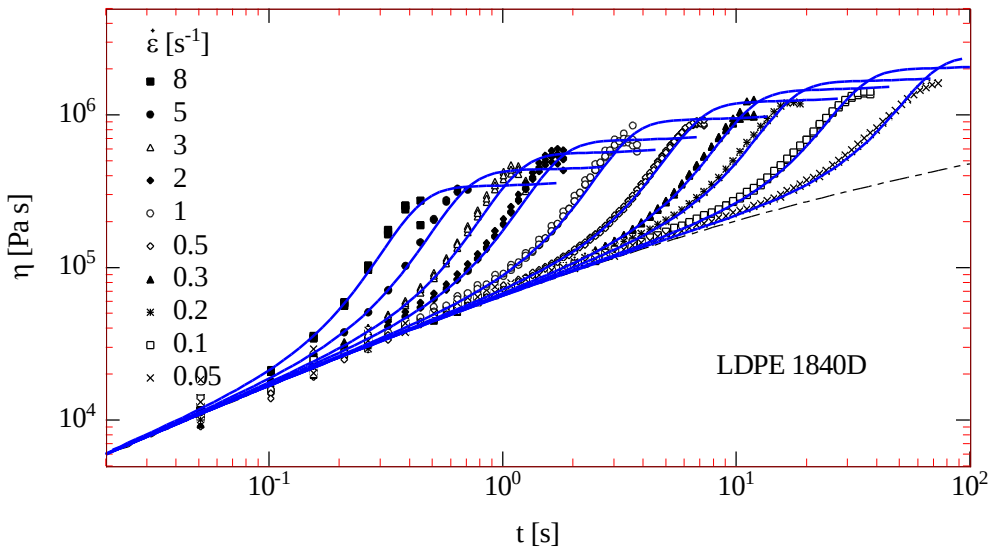


**FIGURE 1.** Elongational viscosity data (symbols) as a function of time for constant strain-rate elongation. Continuous lines indicate predictions of Eq.(1) with non-linear parameters given in Table 2.

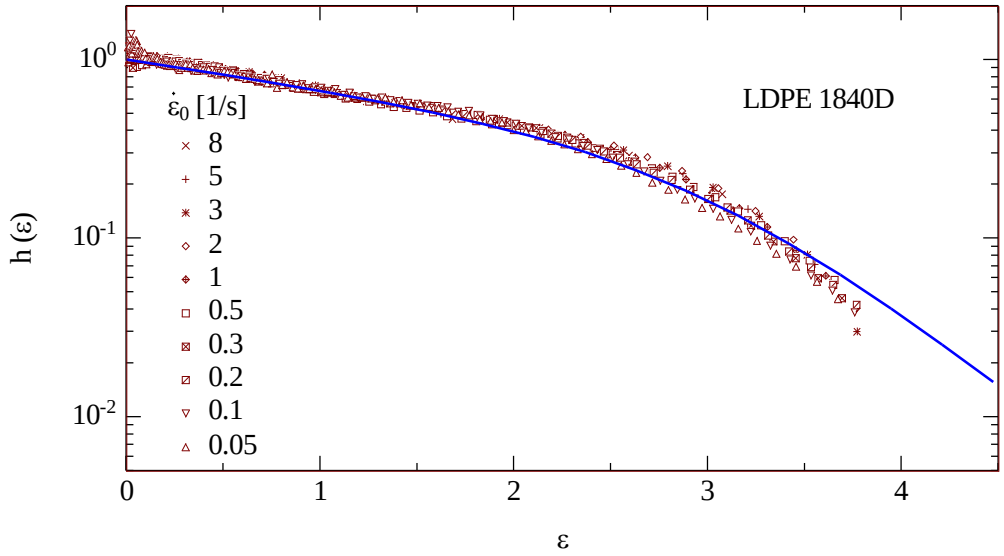


**FIGURE 2.** Damping function of LDPE 1840D calculated from elongational viscosity data (symbols) according to Eq.(6). Continuous line indicates predictions of Eq.(4) with non-linear parameters given in Table 2.

**Experiments at Constant Stress**

The experiments at constant true stress $\sigma_0$, also called creep experiments, were performed in an experimental window of $\sigma_0$ between 5,000 and 70,000 Pa. The Hencky strain $\varepsilon$ as a function of time is presented in Figure 3. Experimental data for LDPE 1840D are presented as discontinuous lines, and predictions of Eq.(7) as continuous lines, respectively. The experimental data are highly reproducible. There is a marked overshoot at the beginning of the experiment due to inertial effects of the rheometer, as already reported earlier[1]. At higher stresses, i.e. at 50,000 and 70,000 Pa, a small second overshoot is also visible.

The start-up of the instrument and the overshoot of the experimental data is more clearly seen when plotting the logarithm of the Hencky strain $\varepsilon$ as function of time (Figure 4). The start-up time increases with increasing stress: it takes 0.7s at 5,000 Pa and 2s at 70,000Pa, before the instrument overcomes the inertial effects and the data show the expected behaviour. Agreement of predictions of Eq.(7) with experimental data is excellent up to stresses of 40,000 Pa. At higher stresses, the significant experimental overshoot causes persistently exaggerated values of the

Hencky strain than predicted by the model. This is clearly a limitation of the experimental set-up, and confirms the findings of our earlier investigation on LDPE 3020D[1].

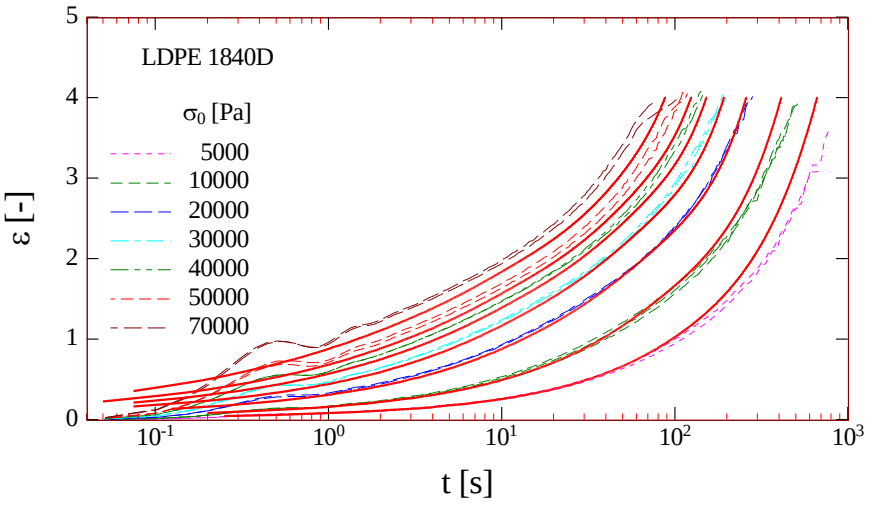


**FIGURE 3.** Hencky strain $\varepsilon$ as function of time for elongation of LDPE 1840D at constant true stress $\sigma_0$. Broken lines represent experimental data. Continuous lines indicate predictions of Eq.(7). True stress $\sigma_0$ is increasing from right to left.

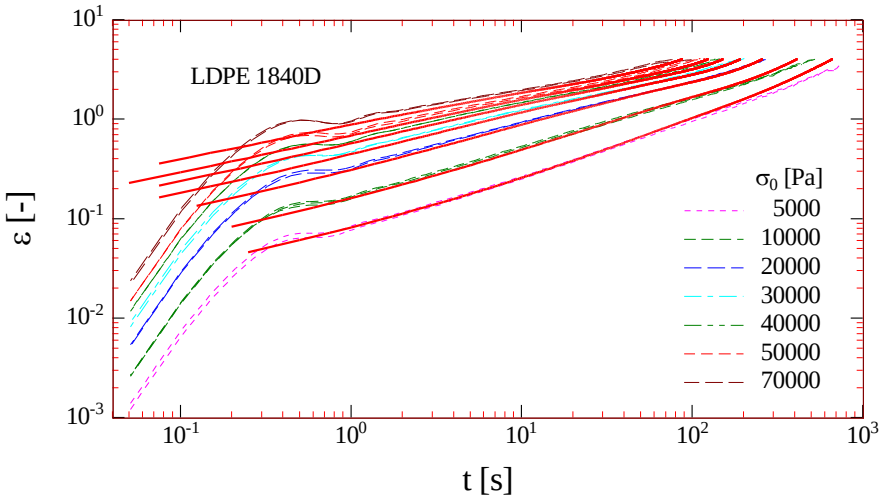


**FIGURE 4.** Logarithm of Hencky strain $\varepsilon$ as function of time for elongation at constant true stress $\sigma_0$. Broken lines represent experimental data for LDPE 1840D. Continuous lines indicate predictions of Eq.(7). True stress $\sigma_0$ is increasing from right to left.

The measured strain rates $\dot{\varepsilon}$ as a function of time are presented for some representative creep experiments in Figure 5, and are compared to predictions of Eq.(7). It is seen that even after the initial overshoot, the measured strain rates oscillate, and the oscillations are the stronger, the

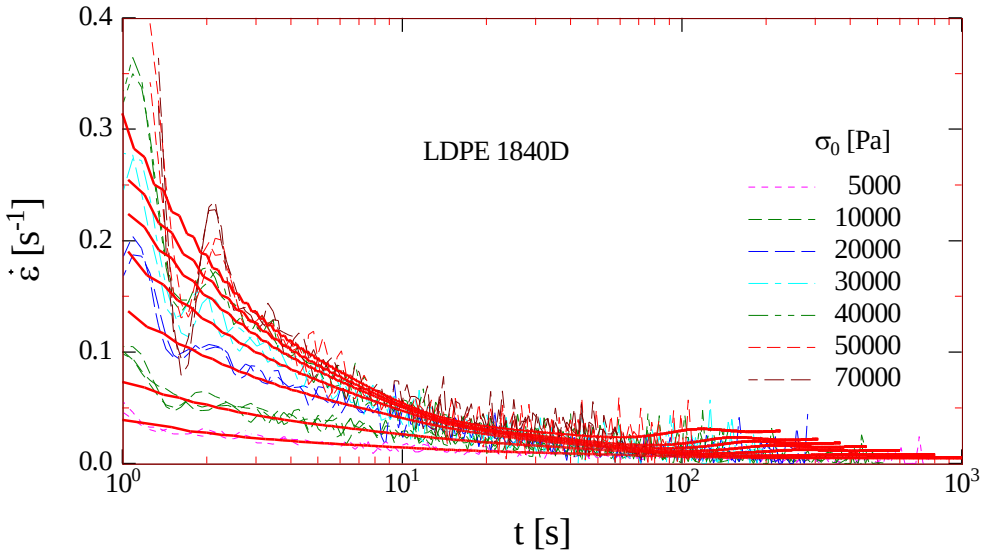


**FIGURE 5.** Strain rate $\dot{\varepsilon}$ as a function of time for elongation at constant true stress $\sigma_0$. Broken lines represent experimental data for LDPE 1840D. Continuous lines indicate predictions of Eq.(7). The true stress $\sigma_0$ is increasing from bottom to top.

higher the imposed stress. As reported earlier[1], this is an effect of the system control of the rheometer: As the strain increases, the torque of the rheometer has to decrease in order to keep the true stress constant. The oscillations are therefore caused by the control loop. The predictions of Eq.(7) describe correctly the average trend of the experimental data. As expected, the strain rate decreases with time, and the decrease is more pronounced for higher stresses imposed.

In Figure 6, the strain rate $\dot{\varepsilon}$ is displayed as a function of time for elongation at constant true stress $\sigma_0$ in a log-log plot for a wider range of stresses, namely from 5,000 to 90,000 Pa and based on predictions of Eq.(7). After the decrease of the strain rate, a minimum is achieved followed by an overshoot. This effect is stronger and occurs earlier for higher values of imposed stress. Subsequent to the overshoot, a constant value of the strain rate is reached.

In correspondence to the elongation rate, which shows a minimum, the elongational viscosity in creep experiments features a maximum, if plotted as a function of time or, as shown in Figure 7, as a function of Hencky strain. The maximum occurs at Hencky strains between 2.5 and 3.5, with the Hencky strain at the maximum increasing with increasing tensile stress, and is followed by a slight undershoot before a steady-state is reached at a Hencky strain of about 6. In elongational experiments, which are limited to strains of 3 or 3.5, this maximum can easily be

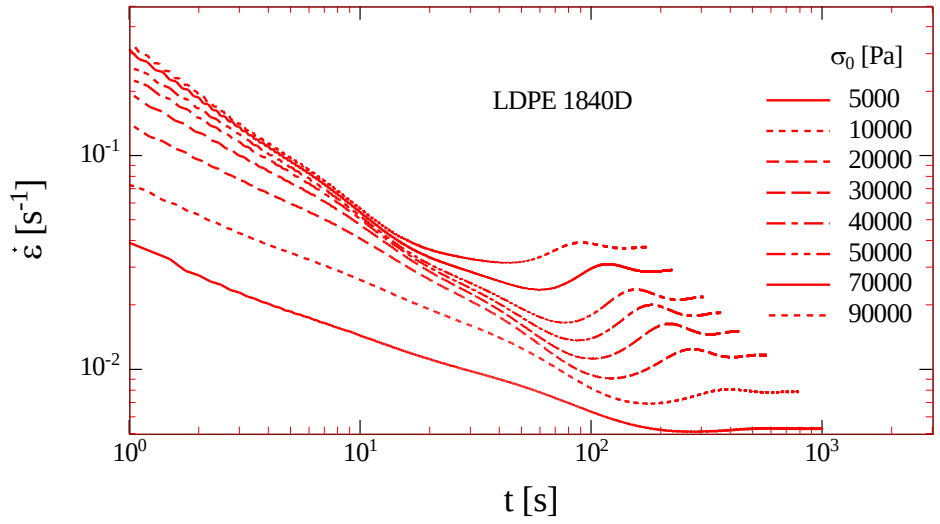


**FIGURE 6.** Predictions of the strain rate $\dot{\varepsilon}$ as a function of time for elongation at constant true stress $\sigma_0$ according to Eq.(7). The true stress $\sigma_0$ is increasing from bottom to top.

confounded with a stationary value of the elongational viscosity, especially if plotted as a function of *t* in a linear plot. However, the true stationary strain rate and the true tensile viscosity are only reached at a considerably higher Hencky strain of the order of 6.

The predicted steady-state elongational viscosities in constant elongation rate and constant tensile stress mode are presented in Figure 8 as a function of the strain rate. As expected,

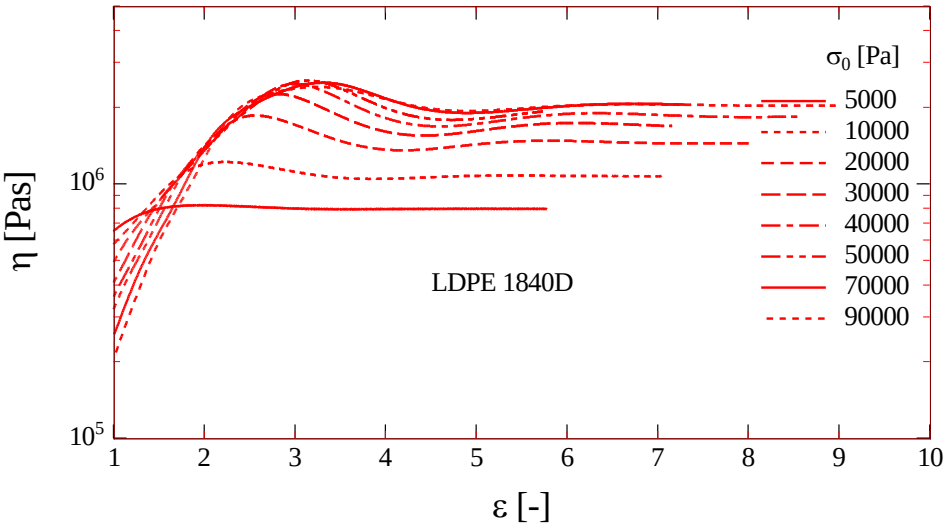


**FIGURE 7.** Prediction of elongational viscosity as a function of Hencky strain $\varepsilon$ for elongation at constant true stress $\sigma_0$ according to Eq.(7).

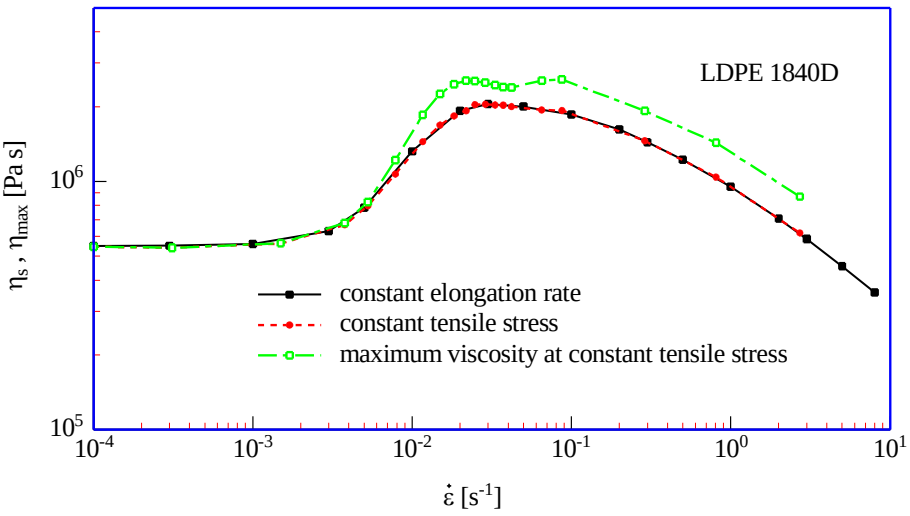


**FIGURE 8.** Prediction of steady-state elongational viscosities as a function of strain rate in constant elongation rate and constant tensile stress mode. The maximum viscosity reached in constant tensile stress mode is also shown.

excellent agreement is found, i.e. the steady-state elongational viscosity can be determined by both constant elongation rate and creep experiments, provided that the measurements extent to large enough Hencky strains. Also shown in Figure 8 is the maximum viscosity reached in

constant tensile stress mode. The difference between steady-state viscosity and maximal viscosity is seen to first increase with increasing viscosity and then to stay constant in the regime of decreasing viscosity, i.e. at higher strain rates, again confirming our earlier results on LDPE 3020D[1].

#### Experiments at Constant Force

Wagner and Rolón-Garrido[29] have already reported results of measurements at constant tensile force using the same low-density polymer melt, which are summarized in the following. The true stress $\sigma$ is plotted as a function of elongation rate $\dot{\varepsilon}$ in Figure 9, with $\sigma_0$ being now the constant engineering stress. Predictions of Eq.(8) with the damping function parameters given in Table 2 are represented by solid lines.

As already reported[29], three different deformation regimes can be identified: In regime 1, the strain rate decreases starting from the maximum value according to Eq.(9). This regime corresponds to elongation at constant true stress, as the cross section of the test sample changes only marginally, and constant engineering stress and constant true stress experiments are nearly equivalent. The steady-state elongational stress as expected for constant tensile stress and constant elongation rate experiments is indicated in Figure 9 by the thick solid line, and the full dots on this line correspond to the constant tensile stresses, which are equivalent to the engineering stresses. At larger values of the engineering stress $\sigma_0$, the experimental data show first an increase of the elongation rate followed by a decrease in correspondence with the start-up behavior of the instrument as already discussed in the case of constant tensile stress experiments.

After having reached a minimum strain rate, the constant tensile force experiment then enters into “regime 2”, where the stress increases by an order of magnitude approximately according to a power law. The exponent of the power law, i.e. the slopes of more or less straight lines in the double-log plot of Figure 9, increases with increasing engineering stress starting from a value close to one.

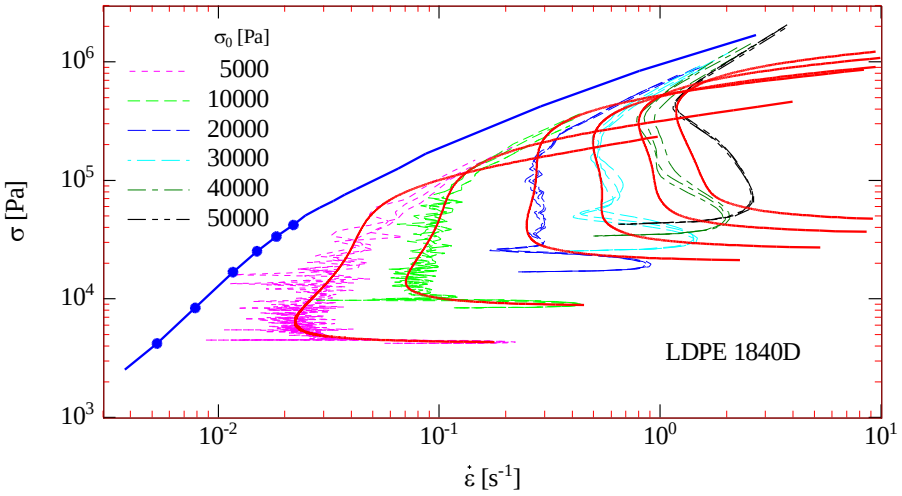


**FIGURE 9.** True stress as function of strain rate $\dot{\varepsilon}$ for constant force elongation with $F_0 = \sigma_0 A_0$. Broken lines represent experimental data for LDPE 1840D. Continuous lines indicate predictions of eq.(7). Engineering stress $\sigma_0$ is increasing from left to right.

Note that in regime 2, the strain rate is approximately constant for larger engineering stresses, and constant force elongation approximates constant elongation rate flow. Regime 2 ends when the viscosity reaches a maximum value[29]. The stress then increase in "regime 3" again according to a power law, however now with an exponent less than one.

It should be noted that the steady-state stress curve as predicted for constant stress and constant elongation rate experiments seems to represent an envelope of the constant tensile force data.

To contrast experiments in constant strain-rate and constant force mode, the elongational viscosity data obtained by experiments performed at constant elongation rate from Figure 1 are compared to predictions of the Wagner-I model according to Eq.(5) by using the nonlinear model parameters (Table 2) obtained by fitting constant tensile force experiments (Figure 10). While the parameter *m* of the model is the same for constant strain rate and constant force mode, significant differences exist for the parameter $\varepsilon_0$. To describe experiments in constant tensile force mode, larger values of $\varepsilon_0$ are needed than in constant strain rate mode, indicating that

constant tensile force experiments reveal a stronger strain hardening potential than constant strain rate experiments. While the start-up of strain hardening is modeled correctly, experimental

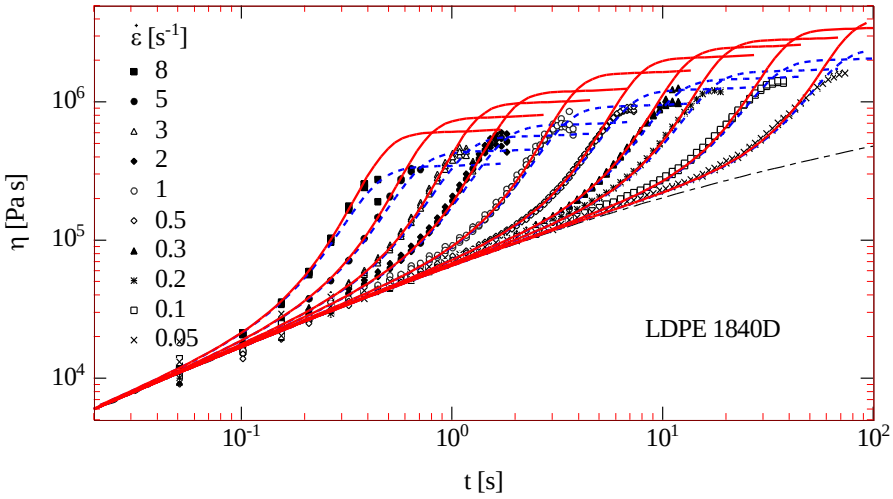


**FIGURE 10.** Elongational viscosity data (symbols) of LDPE 1840D as a function of time for constant strain rate elongation. Continuous and broken lines indicate predictions of Eq.(7) with parameters (Table 2) for constant tensile force and constant strain rate deformation modes, respectively.

elongational viscosity data measured at constant strain rate are clearly lower at larger strains than inferred from constant tensile force experiments.

As seen from Figure 11, deviations between the damping function calculated from experimental data in constant elongation rate experiments and the analytical representation of the damping function according to Eq.(4) with model parameters from constant tensile force experiments, start at Hencky strains of approximately $\varepsilon = 2.5$. Therefore we can conclude that the deviations seen between constant force elongation and constant strain rate elongation are not related to the issue of the existence of a maximum in the constant strain-rate elongational viscosity at Hencky strains of approximately $\varepsilon = 3.5$ and larger as reported by Rasmussen et al.[37].

The underestimation of the effective strain-hardening effect observed in constant strain-rate elongation in comparison to constant tensile force extension may be due to the effect of necking under constant elongation rate conditions. In line with this we note that the difference in the

values of $\varepsilon_0$ (Table 2) between the two modes of operation is smaller for LDPE 1840D than for LDPE 3020D[29]. This may be due to the fact that LDPE 1840D shows for Hencky strains up to 2.4 a stronger strain hardening effect than LDPE 3020D, which may stabilize constant strain-rate flow and delay necking to larger Hencky strains in the case of LDPE 1840D.

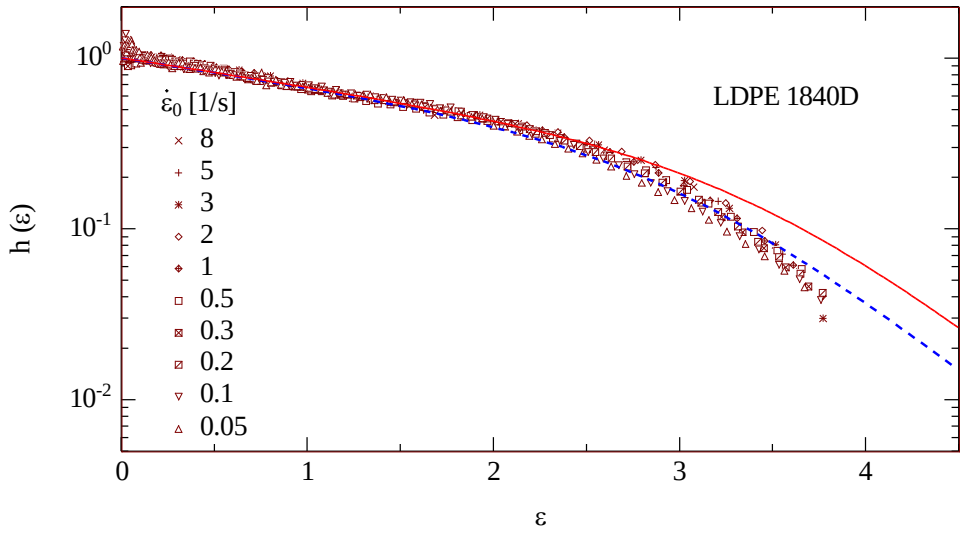


**FIGURE 11.** Damping function calculated from elongational viscosity data (symbols) according to Eq.(6). Continuous and broken lines indicate predictions of Eq.(4) with parameters (Table 2) for constant tensile force and constant strain rate deformation modes, respectively.

## CONCLUSIONS

A full experimental characterization of long-chain branched polyethylene melt 1840D in controlled elongational flows was presented. Within experimental limitations, constant elongational rate, constant tensile stress and constant tensile force experiments can be performed reproducibly by use of a Sentmanat Extensional Rheometer (SER) in combination with an Anton Paar MCR301 rotational rheometer. For the polymer melt investigated here, we found an accessible experimental window of elongational rates of $0.05s^{-1} < \dot{\varepsilon} < 8s^{-1}$ and constant true tensile stresses or engineering stresses in the range of $5{,}000Pa < \sigma_0 < 70{,}000Pa$. Maximum

Hencky strain $\varepsilon$ is limited to $\varepsilon < 4$. While constant strain rate experiments seem to deliver a smooth torque signal, constant true tensile stress tests lead to damped oscillations of the resulting strain rate as well as a marked start-up overshoot of the Hencky strain at higher stresses, which results in persistently exaggerated values of the Hencky strain for the rest of the experiment. In spite of similar state-up effects in the case of constant engineering stress experiments, the instrumental set-up of a torque controlled rheometer seems to be more appropriate for this type of tests as constant force experiments require a constant torque, which confirms earlier results[1]. It is interesting to note that constant force experiments, which can be subdivided in three deformation regimes, comprise some parts of polymer melt characterisation at constant tensile stress and at constant strain rate: The first regime corresponds to constant tensile stress deformation with the elongation rate decreasing from a maximum value to a minimum one, and the second regime approximates constant elongational rate flow. In the third regime, the polymer melts seems to behave as a viscous fluid with a power-law exponent less than one.

The experimental data show time-deformation separability and can be modelled accurately by use of the Wagner I model, i.e. the damping function approach, in all the deformation modes investigated. Predictions of the steady-start elongational viscosity in constant strain rate and creep experiments are found to be identical, albeit only by extrapolation of the experimental data to Hencky strains of the order of 6. For constant stress experiments, a minimum in the strain rate and a corresponding maximum in the elongational viscosity are predicted at a Hencky strain of the order of 3, which, although larger than the steady-state value, follows roughly the general trend of the steady-state elongational viscosity.

This constitutive analysis of elongational data for LDPE 1840D confirms earlier findings for another LDPE melt, LDPE 3020D[1]. It also confirms conclusively that constant tensile force experiments indicate a larger strain hardening potential than seen in elongational rate or constant tensile stress experiments. This may be indicative of the effect of necking under constant elongation rate or constant tensile stress conditions according to the Considère criterion, an issue that it deserves more attention in future works.

**ACKNOWLEDGEMENTS**

Financial support by the German Science Foundation (DFG) is gratefully acknowledged.

**REFERENCES**

1. Wagner, M.; Rolón-Garrido V.H. In Novel Trends in Rheology V; Zatloukal M. Ed.; AIP Conference Proceedings 1526: Zlín, 2013; pp 168-183.
2. Bach, A.; Almdal, K.; Rasmussen, H.K.; Hassager O., *Macromolecules* **2003**, 36, 5174-5179.
3. Auhl, D.; Stange, J.; Münstedt, H.; Krause, B.; Voigt, D.; Lederer, A.; Lappan, U.; Lunkwitz, K., *Macromolecules* **2004**, 37, 9465-9472.
4. Stadler, F.J.; Kaschta, J.; Münstedt, H.; Becker, F.; Buback, M., *Rheol. Acta* **2009**, 48, 479-490.
5. Rolón-Garrido, V.H.; Luo, J.; Wagner, M.H., *Rheol. Acta* **2011**, 50, 519-535.
6. Yamaguchi, M.; Suzuki, K., *J. Appl. Polym. Sci.* **2002**, 86, 79-83.
7. Spitael, P.; Macosko, C.W., *Polym. Eng. Sci.* **2004**, 44, 2090-2100.
8. Münstedt, H.; Steffl, T.; Malmberg, A., *Rheol. Acta* **2005**, 45, 14-22.
9. Stange, J.; Münstedt, H., *J. Rheol.* **2006**, 50, 907-923.
10. Stadler, F.J.; Nishioka , A.; Stange, J.; Koyama, K.; Münstedt, H., *Rheol Acta* **2007**, 46, 1003–1012.
11. Cogswell, F.N., *Plastics and Polymers* **1968**, 36, 109-111.
12. Cogswell, F.N., *Appl. Polym. Symp.* **1975**, 27, 1-18.
13. Vinogradov ,G.V.; Fikhman, V.D.; Radushkevich, B.V., *Rheol. Acta* **1972**, 11, 286-291.
14. Laun, H.M.; Münstedt, H.; *Rheol. Acta* **1976**, 15, 517-524.
15. Meissner, J., *Trans. Soc. Rheol.* **1972**, 16(3), 405-420.
16. Münstedt, H., *Rheol. Acta* **1975**, 14, 1077-1088.
17. Kurzbeck, S.; Oster, F.; Münstedt, H.; Nguyen, T.Q.; Gensler, R.; *J. Rheol.* **1999**, 43(2), 359-374.
18. Rolón-Garrido, V.H.; Resch, J.A.; Wolff, F.; Kaschta, J.; Münstedt, H.; Wagner, M.H., *Rheol Acta* **2011**, 50, 645–653.
19. Andrade, R.J.; Maia, J.M., *J. Rheol.* **2011**, 55(5), 925-937.
20. Meissner, J., *Rheol. Acta* **1971**, 10, 230-242.
21. Wagner, M.H.; Bernnat A.; Schulze, V., *J. Rheol.* **1998**, 42(4), 917-928.
22. Wagner, M.H.; Bastian, H.; Bernnat, A.; Kurzbeck S.; Chai, C.K., *Rheol Acta* **2002**, 41, 316–325.
23. Muke, S.; Ivanov, I.; Kao, N.; Bhattacharya, S.N., *J. Non-Newtonian Fluid Mech.* **2001**, 101, 77-93.
24. Petrie, C.J.S., *J. Non-Newtonian Fluid Mech.* **1977**, 2, 221-253.
25. Chang, H.; Lodge, A.S., *Rheol. Acta* **1971**, 10, 448-449.
26. Petrie, C.J.S., *Rheol. Acta* **1995**, 34, 12-26.
27. Szabo, P.; McKinley, G.H.; Clasen, C., *J. Non-Newtonian Fluid Mech.* **2012**, 169, 26-41.
28. Raible, T.; Stephenson, S.E.; Meissner, J.; Wagner, M.H., *J. Non-Newtonian Fluid Mech.* **1982**, 11, 239-256.

29. Wagner, M.H.; Rolón-Garrido, V.H., *J. Rheol.* **2012**, 56(5), 1279-1297.
30. Sentmanat, M., *Rheol. Acta* **2004**, 43, 657-669.
31. Rolón-Garrido, V.H.; Wagner, M.H., *Rheol. Acta* **2009**, 48(3), 245-284.
32. Aho, J.; Rolón-Garrido, V.H.; Syrjälä, S.; Wagner, M.H., *Rheol. Acta* **2010**, 49, 359–370.
33. Aho, J.; Rolón-Garrido, V.H.; Syrjälä, S.; Wagner, M.H., *J. Non-Newtonian Fluid Mech.* **2010**, 165, 212–218.
34. Wagner, M.H., R*heol. Acta* **1976**, 15, 136-142.
35. Wagner, M.H., *Rheol. Acta* **1979**, 18(6), 681-692.
36. Wagner, M.H., *J. Non-Newton. Fluid Mech.* **1978**, 4, 39-55.
37. Rasmussen, H.K.; Nielsen, J.K.; Bach, A.; Hassager, O., *J. Rheol.* **2005**, 49, 369-381.